Synthesis and characterization of 10Sc1CeSZ powders prepared by a solid–liquid method for electrolyte-supported solid oxide fuel cells

Man Liu, Chang Rong He, Wei Guo Wang*, Jian Xin Wang*

Division of Fuel cell and Energy Technology, Ningbo Institute of Material, Technology & Engineering, Chinese Academy of Sciences, Ningbo 315201, PR China

Abstract

10Sc1CeSZ is one of the most important electrolyte materials used for solid oxide fuel cells (SOFCs). A novel solid–liquid method (SLM) was adopted for the preparation of 10Sc1CeSZ nanopowder. High-purity, single-phase, homogeneous 10Sc1CeSZ powder was successfully prepared using this method. The resulting powders and ceramic pellets were characterized by X-ray diffraction (XRD), scanning electron microscopy (SEM) and electrochemical impedance spectroscopy (EIS). A cubic structure was obtained when the value of the specific surface area (SSA) of the starting material ZrO_2 was greater than $60\ m^2\ g^{-1}$. A conductivity of $0.14\ S\ cm^{-1}$ at 800 °C was achieved for the sintered pellets. The performance of the electrolyte-supported cell (ESC) $NiO + GDC/10Sc1CeSZ/10Sc1CeSZ + LSM$ reached $0.66\ W\ cm^{-2}$ at 0.75 V and 850 °C.
© 2013 Elsevier Ltd and Techna Group S.r.l. All rights reserved.

Keywords: Solid–liquid method; Oxide ionic conductivity; 10Sc1CeSZ; Solid oxide fuel cells

1. Introduction

Solid oxide fuel cells (SOFCs), a high-efficiency and clean power generation technology, have been used in a broad range of applications from small auxiliary power units to large-scale power plants [1,2]. The electrolyte is the core part of the SOFCs, the main function of which is to conduct ions and isolate air and fuel. The performance of the electrolyte determines the performance of the SOFCs. For electrolyte-supported SOFCs, the mechanical properties and the conductivity of the electrolyte are particularly important in comparison with that of anode-supported SOFCs [3]. Among zirconia-based electrolytes, scandia-stabilized zirconia (ScSZ) is a promising candidate because it exhibits appropriate thermal expansion, good mechanical properties and the highest oxide ionic conductivity due to the similar ionic radius of the Sc^{3+} dopant to that of the Zr^{4+} host ($R = r\ Sc^{3+}/r\ Zr^{4+} = 1.03$) [4,5]. Generally speaking, dopants, such as CeO_2 [6–11], Y_2O_3 [12–16], Yb_2O_3 [17] and Al_2O_3 [18], are helpful in stabilizing the cubic phase structure of ScSZ electrolytes down to room temperature. A sample with 10 mol% Sc_2O_3 and 1 mol% CeO_2 (10Sc1CeSZ) exhibits the best oxide ionic conductivity and good stability during the

extended annealing period [10,11]. In previous studies, 10Sc1CeSZ powders were synthesized by several methods, including solid-state reaction [19], co-precipitation [8,17,20], sol–gel [21] process and polymeric precursor method [11]. To obtain 10Sc1CeSZ ceramics with good properties, an initial powder with good dispersion and high reactivity is required. In this work, a novel solid–liquid method (SLM) was adopted for the preparation of 10Sc1CeSZ nanopowder. This method is attractive for producing powders with multicomponents, as it can ensure uniform mixing of the three elements. The improved SLM method uses ZrO_2 with large S_{BET} as the solid form, whereas $Sc(NO_3)_3$ and $Ce(NO_3)_3$ are in the liquid form. This article first introduces a detailed procedure and later studies the effect of the SSA of the starting material on the crystal form of 10Sc1CeSZ, the effect of the experimental conditions on powder morphology and finally, presents the ionic conductivity of the sintered pellets and the performance of the ESC ($NiO + GDC/10Sc1CeSZ/10Sc1CeSZ + LSM$).

2. Experiments

2.1. Powder synthesis

High-purity $Ce(NO_3)_3 \cdot 6H_2O$, $Zr(OH)_4$, HNO_3, citric acid (CA) and acrylic acid (AA) were used as starting materials as

*Corresponding authors. Tel: +86 574 87911363; fax: +86 574 87910728.
E-mail addresses: wgwang@nimte.ac.cn (W.G. Wang),
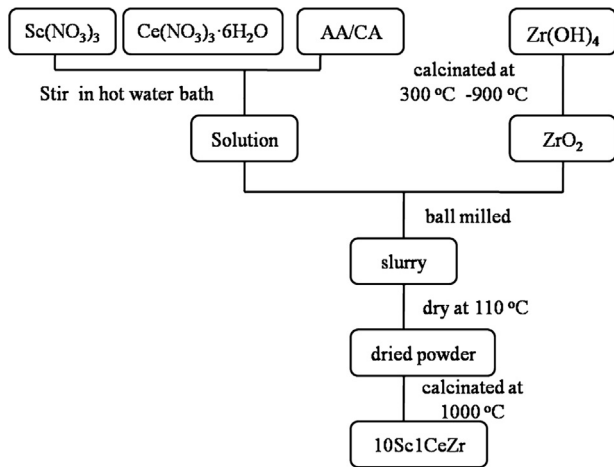jxwang@nimte.ac.cn (J.X. Wang).

Fig. 1. Flow chart of the 10Sc1CeSZ synthesis by SLM.

purchased from Sinopharm Chemical Reagent Co., Ltd. Sc_2O_3 was purchased from Hunan Oriental Scandium Co., Ltd. of China.

A flow chart of the SLM method used to prepare 10Sc1CeSZ powders is shown in Fig. 1. ZrO_2 powders were obtained from the calcination of $Zr(OH)_4$ at different temperatures from 300 °C to 900 °C. $Sc(NO_3)_3$ solution was prepared by dissolving Sc_2O_3 in hot nitric acid. The slurry was prepared by adding the required quantity of $Ce(NO_3)_3 \cdot 6H_2O$, CA or AA, ZrO_2 to the $Sc(NO_3)_3$ solution. The uniformity of the slurry was ensured by planetary ball milling for 24 h. The homogeneous slurry was dried at 110 °C and was calcined at1000 °C.

2.2. Powder characterization

TGA/DTA analysis at the temperature range of 30–900 °C was conducted with a heating rate of $5 \, °C \cdot min^{-1}$ in air. The phase structures of the powders were characterized using XRD, and the data were collected using a Bruker D8 Advance (Germany) with Cu Kα radiation at a step of $0.02° \, s^{-1}$ in the range of 2θ from 20° to 80°. The morphology of the powder was observed by SEM (Hitachi, S-4800, Japan). The morphology of the sintered pellet was observed by Desktop SEM (Hitachi, TM-1000, Japan). The oxide ionic conductivity of the pellets was measured using a frequency response analyzer (FRA, Solartron 1260) over a frequency range of 0.1 Hz–1 MHz over a temperature range of 450–850 °C in air with Pt electrodes. The ionic conductivity, σ, was calculated from the impedance data, and the activation energy (E_a) of the conductivity was determined by the Arrhenius law:

$$\sigma T = \sigma_o \exp(-E_a/kT),$$

where σ_0 is the pre-exponential factor and k is the Boltzmann constant. The structural features were characterized by Perkin-Elmer FT-IR spectroscopy using KBr pellet method in the range of $500–4000 \, cm^{-1}$. The SSA of the powders was measured by the Brunauer Emmett Teller (BET) isotherm technique with nitrogen adsorption (V-sorb 2800P, China).

2.3. Cell fabrication and testing

Electrolyte supported cells with the configuration of NiO+GDC/10Sc1CeSZ/LSM+10Sc1CeSZ were fabricated. The 10Sc1CeSZ powder used in the support and cathode was fabricated by the SLM method mentioned above.

10Sc1CeSZ electrolyte substrates with a thickness of approximately 250 μm were fabricated by the tape-casting method and were sintered at 1550 °C for five hours. To prepare the anode, an NiO–GDC suspension was prepared with mixed powders of NiO (60 wt%) and GDC (40 wt%) by ball milling with zirconia balls. The anode suspension was coated on the 10Sc1CeSZ electrolyte substrates via screen printing. The LSM-10Sc1CeSZ (mass ratio50:50) cathode suspension was prepared and screen printed on the other side of the electrolyte substrates. The cells were co-sintered at 1100 °C to investigate the performance. The active area was 4 cm by 4 cm.

The ESCs (active area: $16 \, cm^2$) were coated with NiO paste on the anode and Ag paste on the cathode for current collection, reduced at 850 °C and tested at 850 °C and 830 °C in a stainless steel test-house. Dry hydrogen was used as a fuel and air as an oxidant.

3. Results and discussion

The XRD patterns of the 10Sc1CeSZ powders prepared using ZrO_2 calcined from $Zr(OH)_4$ under different temperatures are shown in Fig. 2. The 10Sc1CeSZ powders were labeled as ZrO_2-300 to ZrO_2-900 according to the calcination temperature of $Zr(OH)_4$. All 10Sc1CeSZ powder samples were calcined at 1000 °C for 2 h. For three powders, ZrO_2-300, ZrO_2-400 and ZrO_2-500, only the pure cubic phase were observed, whereas for the powders of ZrO_2-600, ZrO_2-700 and ZrO_2-800, ZrO_2-900, in addition to the cubic phase, the tetragonal and monoclinic phases were also observed in the XRD patterns. The crystalline structures of the 10Sc1CeSZ powders and the S_{BET} value of the ZrO_2 obtained from $Zr(OH)_4$ calcined at different temperatures are listed in Table 1.
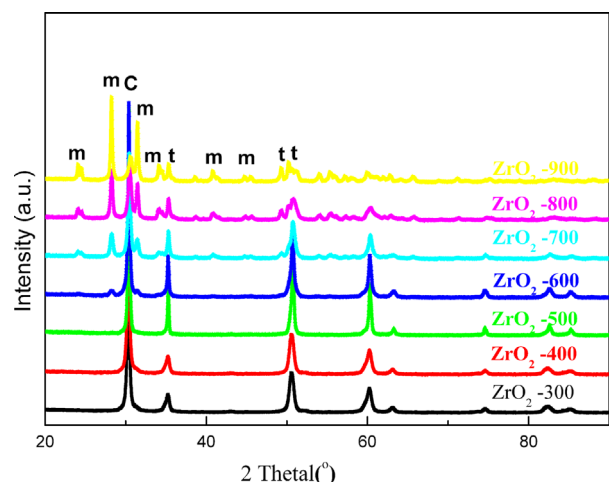

Fig. 2. XRD patterns of the 10Sc1CeSZ powders using ZrO_2-300 to ZrO_2-900 as the starting material (ZrO_2-300, means ZrO_2 was obtained from $Zr(OH)_4$ calcined at 300 °C).

Table 1
S_{BET} of ZrO_2 obtained from $Zr(OH)_4$ calcined at different temperatures and crystalline structures of the 10Sc1CeSZ powders.

Calcination temperature of $Zr(OH)_4$ (°C)	Specific surface area of ZrO_2 (m²/g)	Crystalline structure of 10Sc1CeSZ
300	300	c
400	118	c
500	62.6	c
600	50.4	c+m
700	30.5	c+m
800	17.7	c+m+t
900	10.2	c+m+t

c: Cubic Phase; m: Monoclinic Phase; t:Tetragonal Phase.
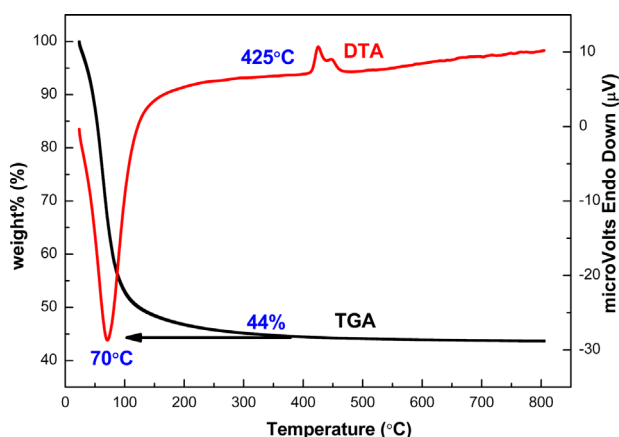
Fig. 3. TGA-DTA thermal analysis curves of the $Zr(OH)_4$ sample.

Fig. 4. XRD patterns of the 10Sc1CeSZ powders by the SLM method calcined at 500 °C, 600 °C, 700 °C, and 800 °C.

Fig. 2 shows that the intensity of the cubic phase rises with the increasing S_{BET} of ZrO_2. Smaller ZrO_2 particles with larger S_{BET} show higher reaction activity, as a result, it will be propitious for the doping elements Sc and Ce to solid-state diffuse into the ZrO_2 crystal lattice and form a 10Sc1CeSZ solid-solution at lower temperatures, such as 500 °C. For S_{BET} of ZrO_2 above 60 m² g^{-1}, the product 10Sc1CeSZ is in the single cubic phase. In conclusion, a calcination temperature of $Zr(OH)_4$ of 500 °C or below is advantageous for the formation of pure cubic phase 10Sc1CeSZ.

To determine the appropriate calcination temperature of $Zr(OH)_4$, TGA/DTA thermal analysis was conducted as shown in Fig. 3. The loss in weight of approximately 44% for the TGA curve was due to $Zr(OH)_4$ dehydrated to ZrO_2 accompanied by the sharp endothermic reaction in DTA curve. The exothermic peak approximately 425 °C in the DTA curve was due to the transformation of amorphous zirconia to monoclinic zirconia. With an increase of temperature, no further changes in weight and heat were detected, indicating that ZrO_2 was in a relatively stable state. Combined with the results given by Table 1 and Fig. 2, ZrO_2-500 is the best choice. Future references to the powder in this article refer to ZrO_2-500 as the raw material.

The XRD patterns of the 10Sc1CeSZ powders calcined at different temperatures from 500 to 800 °C are shown in Fig. 4. All four powders were in the pure cubic phase. The temperature at which the pure cubic phase of 10Sc1CeSZ is formed can be as low as 500 °C, which is comparable to the traditional co-precipitation method. The peak intensity increases and the
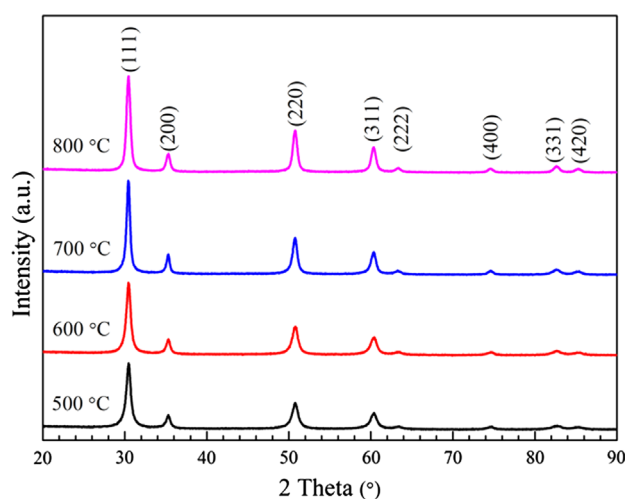
peak width narrows as the calcination temperature getting higher which indicated the crystalline grain growth and the improvement of the crystallization degree.

To obtain insight into the effect of CA/AA addition, FT-IR spectra were obtained for 10Sc1CeSZ precursors with and without CA/AA addition, as shown in Fig. 5. The waveform, wave intensity and peak position of the characteristic peaks of the three samples are consistent, indicating that a chelating reaction does not occur between CA/AA and the metal ions. The fact that no color change of the solution was found with the addition of CA/AA also indicates that CA/AA played a physical effect. CA/AA addition adjusts the viscosity of the slurry, which guarantees the uniformity. The function of CA/AA is to act as a physical barrier effect of powder particles in the early calcination process. SEM images were taken to identify the influence of CA/AA and are shown in Fig. 6. With the addition of CA or AA, the morphology of the powder is improved and agglomeration is restrained. Especially for AA addition, homogeneous particles were obtained and aggregation was minimal. AA played a significant role in the formation of the 3D network during the process of calcination, which was attributed to the co-operation of the carboxyl group and the ethylenic bond. The function and advantage of AA addition during the process of powder preparation was studied and discussed in detail by Liu [22].
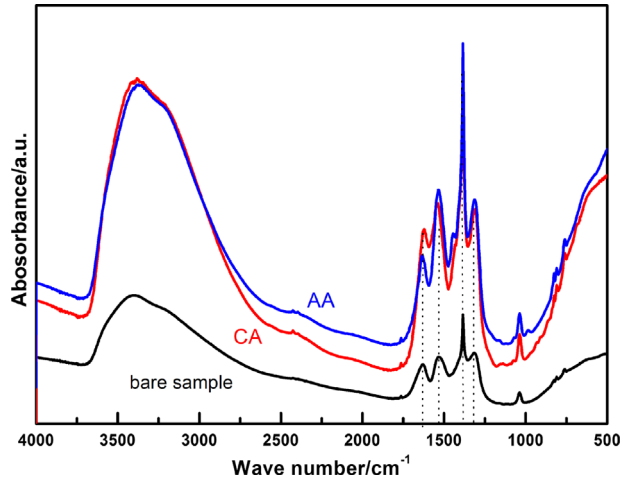
Fig. 5. FT-IR spectra of the 10Sc1CeSZ precursors: (a) bare sample; (b) with CA addition and (c) with AA addition.

The heating rate also has a great effect on the morphology of the powders. Fig. 7 shows the representative SEM images of 10Sc1CeSZ prepared at different heating rates: $0.5\ ^{\circ}\text{C min}^{-1}$, $1\ ^{\circ}\text{C min}^{-1}$ and $2\ ^{\circ}\text{C min}^{-1}$. Decreasing the heating rate to $0.5\ ^{\circ}\text{C min}^{-1}$, the particles are well dispersed. As the heating rate rises to $1\ ^{\circ}\text{C min}^{-1}$, particles tend to agglomerate. As the heating rate reaches $2\ ^{\circ}\text{C min}^{-1}$, agglomeration becomes more intensive. The best morphology is achieved as shown in Fig. 7(a).

The 10Sc1CeSZ powders obtained from the SLM method were then pressed into a pellet of 8 mm diameter and 1.0 mm thickness under a pressure of 300 MPa and were then sintered at 1500 °C for 5 h. The photograph of the surface and the fracture surface of 10Sc1CeSZ sintered pellets is shown in Fig. 8. The pellet was nearly fully dense with very few obturators in the grain. The well-developed grain boundary and the very low porosity are typical micro-structural features of ceramics in the final stage of sintering. The network formed in
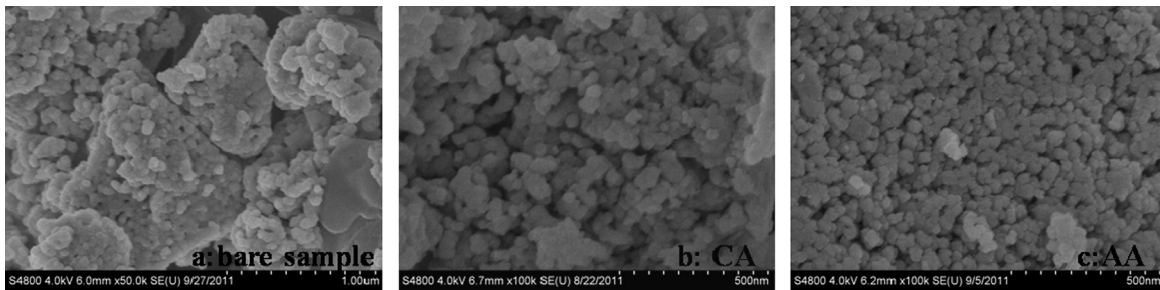

Fig. 6. SEM images of the 10Sc1CeSZ powders: (a) bare sample; (b) with CA addition and (c) with AA addition.
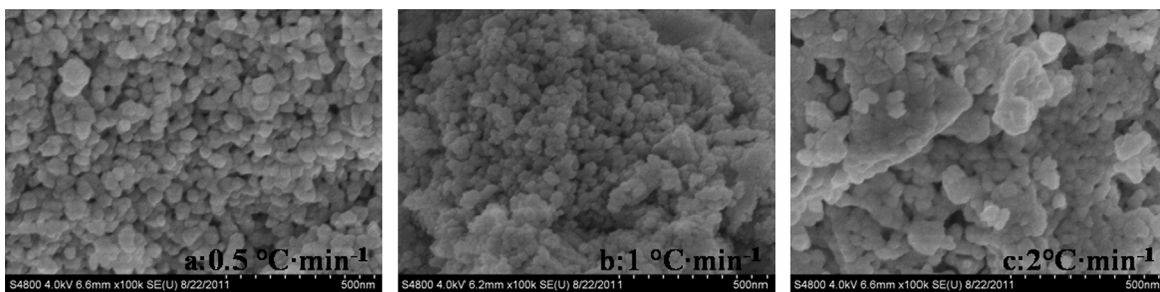

Fig. 7. SEM images of the 10Sc1CeSZ calcined under different heating rates: (a): $0.5\ ^{\circ}\text{C}\cdot\text{min}^{-1}$; (b): $1\ ^{\circ}\text{C}\cdot\text{min}^{-1}$ and (c): $2\ ^{\circ}\text{C}\cdot\text{min}^{-1}$.
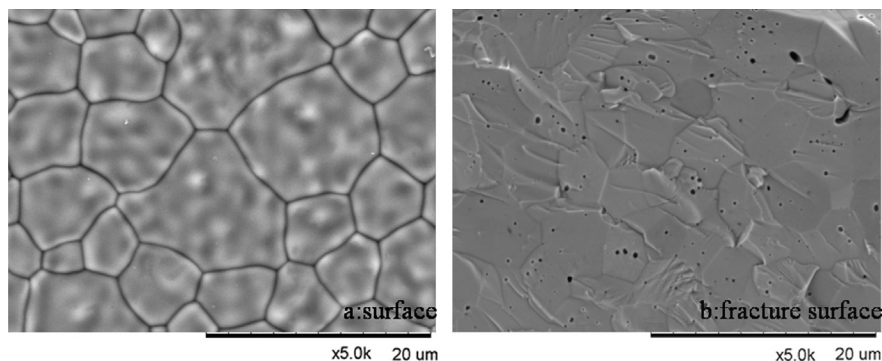

Fig. 8. Photographs of the of 10Sc1CeSZ pellet sintered at 1500 °C (a) surface and (b) fracture surface.

the heating process by AA ensures the homogeneity of the solution, which restrains the agglomeration and assures that doping elements dissolve into the lattice structure of the ZrO_2 matrix evenly. As the particle size is kept in a narrow range, the body shrinks uniformly, and porosity is reduced during the sintering process of the electrolyte film. The SLM method increases the sintering activity of the powder and improves the microstructure of the electrolyte film.

Fig. 9 shows the Arrhenius plot for the sintered pellets. Compared with the co-precipitation method we previously explored and reported on [8], the oxide ionic conductivity of pellets prepared by the SLM method is much higher over the whole investigation temperature range from 500 to 900 °C. This indicates a lower Ea for ion conduction and a larger driving force for the sintering and grain growth. Less porosity in the lattice leads to a more compact grain boundary and a higher conductivity. The ionic conductivity of 10Sc1CeSZ sintered pellets is between 0.12 and 0.13 S cm^{-1} at 800 °C, and the best sample reaches 0.14 S cm^{-1}.

Finally, the performance of the single cell (NiO+GDC/10Sc1CeSZ /LSM+10Sc1CeSZ) is shown in Fig. 10. The cell
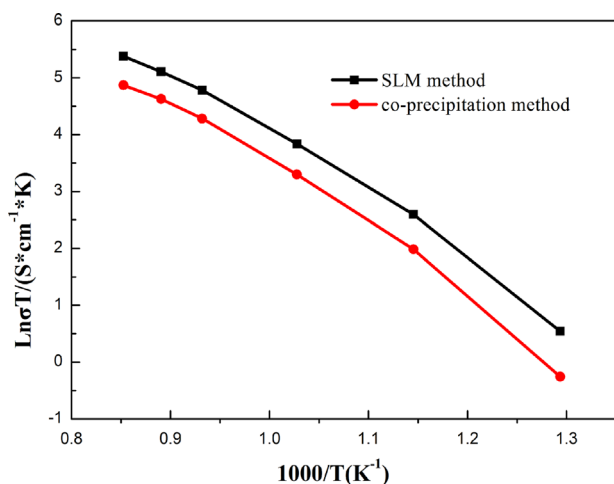
exhibited OCVs of 1.128 V and 1.152 V at 850 °C and 830 °C, respectively. The open cell voltage reached 1.10 V, which indicates a tight electrolyte, good cell sealing and optimal electrical potential through the cell. The curves exhibited a power density of 0.66 W cm^{-2} at 850 °C and 0.62 W cm^{-2} at 830 °C (H$_2$/air, 0.75 V, active electrode area of 16 cm^2). The testing results showed that good performance was achieved for ESC.

4. Conclusions

In this work, 10Sc1CeSZ was successfully synthesized by an SLM method and was characterized. The optimal condition is high-reactivity ZrO_2 (S$_{BET}$ above 60 m^2 g^{-1}) as the starting material and AA as an addition agent with a heating rate of 0.5 °C min^{-1}. Process optimization led to high-purity, homogeneous, spherical, single pure cubic phase 10Sc1CeSZ powders. The ionic conductivity of the sintered 10Sc1CeSZ sample from the SLM method reached 0.14 S cm^{-1} at 800 °C, which suggests a good candidate for SOFCs. The SLM method exhibited good properties for microstructure, sintering ability and conductivity. The performance of the ESC reached 0.66 W cm^{-2} at 0.75 V and 850 °C. These results indicated that the SLM method is an excellent technique for the synthesis of 10Sc1CeSZ powders with good performance. Given the advantages and convenience of this method, it can be applied to the preparation of other types of oxide powders.

Acknowledgments

Fig. 9. The Arrhenius plot for the sintered pellets by the SLM method and the co-precipitation method.
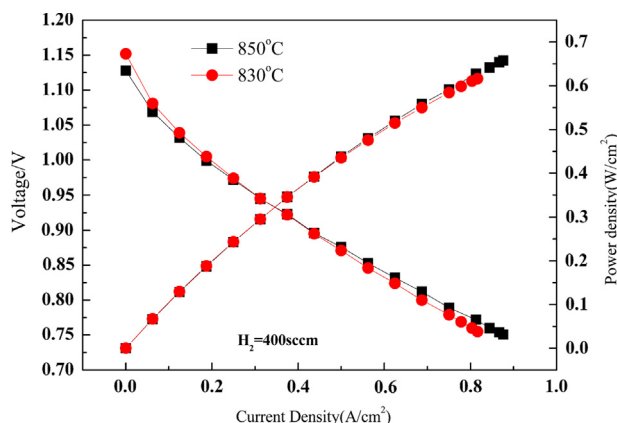
Fig. 10. *I–V* curves of the ESC (NiO+GDC/10Sc1CeSZ /LSM+10Sc1CeSZ) at 850 °C and 830 °C.

References

[1] Y. Mizutani, K. Hisada, K. Ukai, H. Sumi, M. Yokoyama, Y. Nakamura, O. Yamamoto, From rare earth doped zirconia to 1 kW solid oxide fuel cell system, J. Alloy. Compd. 408–412 (2006) 518–524.

[2] B. Lin, S. Wang, X. Liu, G. Meng, Simple solid oxide fuel cells, J. Alloy. Compd. 490 (2010) 214–222.

[3] C. Guo, J. Wang, C. He, W.G. Wang, Effect of alumina on the properties of ceria and scandia co-doped zirconia for electrolyte-supported SOFC, Ceram. Int. 39 (8) (2013) 9575–9582.

[4] D.-S. Lee, W.-S. Kim, S.-H. Choi, J. Kim, H.-W. Lee, J.-H. Lee, Characterization of ZrO$_2$ co-doped with Sc$_2$O$_3$ and CeO$_2$ electrolyte for the application of intermediate temperature SOFCs, Solid State Ionics 176 (2005) 33–39.

[5] H. Huang, C.-H. Hsieh, N. Kim, J. Stebbins, F. Prinz, Structure, local environment, and ionic conduction in scandia stabilized zirconia, Solid State Ionics 179 (2008) 1442–1445.

[6] J.W. Fergus, Eletrolytes for solid oxide fuel cells, J. Power Sources 162 (2006) 30–40.

[7] S.P.S. Badwal, F.T. Ciacchi, D. Milosevic, Scandia–zirconia electrolytes for intermediate temperature solid oxide fuel cell operation, Solid State Ionics 136–137 (2000) 91–99.

[8] M. Liu, C. He, J. Wang, W.G. Wang, Z. Wang, Investigation of $(CeO_2)_x(Sc_2O_3)_{(0.11-x)}(ZrO_2)_{0.89}$ ($x=0.01-0.10$) electrolyte material for intermediate-temperature solid oxide fuel cells, J. Alloy. Compd. 502 (2010) 319–323.

[9] Y. Arachi, T. Asai, O. Yamamoto, Y. Takeda, N. Imanishi, K. Kawate, C. Tamakoshi, Electrical conductivity of $ZrO_2-Sc_2O_3$ doped with HfO_2, CeO_2, and Ga_2O_3, J. Electrochem. Soc. 148 (2001) A520–A523.

[10] Z.W. Wang, M.J. Cheng, Y.L. Dong, M. Zhang, Anode-supported SOFC with 1Ce10ScZr modified cathode/electrolyte interface, J. Power Sources 156 (2006) 306–310.

[11] H. Tu, X. Liu, Q. Yu, Synthesis and Characterization of scandia ceria stablized zirconia powders prepared by polymeric precursor method for integration into anode-supported solid oxide fuel cells, J. Power Sources 196 (2011) 3109–3113.

[12] S.P.S. Badwal, F.T. Ciacchia, S. Rajendran, J. Drennan, An investigation of conductivity, microstructure and stability of electrolyte compositions in the system 9 mol% $(Sc_2O_3 - Y_2O_3)$–ZrO_2 (Al_2O_3), Solid State Ionics 109 (1998) 167–186.

[13] D. Meyer, U. Eisele, R. Satet, J. Rödel, Codoping of zirconia with yttria and scandia, Scripta Mater. 58 (2008) 215–218.

[14] Y.W. Zhang, X. Sun, G. Xu, S.J. Tian, C.S. Liao, C.H. Yan, Co-doping effects of Y^{3+} and Sc^{3+} on the crystal structures, nanoparticle properties and electrical behavior of ZrO_2 solid solutions prepared by a mild urea-based hydrothermal method, Phys. Chem. Chem. Phys. 5 (2003) 2129–2134.

[15] J.T.S. Irvine, J.W.L. Dobson, T. Politova, S.G. Martin, A. Shenouda, Co-doping of scandia-zirconia electrolytes for SOFCs, Faraday Discuss 134 (2007) 41–49.

[16] T.I. Politova, J.T.S. Irvine, Investigation of scandia–yttria–zirconia system as an electrolyte material for intermediate temperature fuel cells —influence of yttria content in system $(Y_2O_3)_x(Sc_2O_3)_{(11-x)}(ZrO_2)_{89}$, Solid State Ionics 168 (2004) 153–165.

[17] Y. Fang, J. Wang, H. Miao, C. Guo, W.G. Wang, Investigation of the crystal structure and ionic conductivity in the ternary system $(Yb_2O_3)_x - (Sc_2O_3)_{(0.11-x)} - (ZrO_2)_{0.89}$ ($x=0-0.11$), J. Alloy. Compd. 549 (2013) 200–205.

[18] T. Ishii, Structural phase transition and ionic conductivity in $0.88ZrO_2 - (0.12-x)Sc_2O_3 - xAl_2O_3$, Solid State Ion. 78 (1995) 333–338.

[19] R. Ruh, H.J. Garrett, R.F. Domagala, V.A. Patel, The system zirconia-scandia, J. Am. Ceram. Soc. 60 (1977) 399–403.

[20] S.P.S. Badwal, J. Drennan, Microstructure/conductivity relationship in the scandia–zirconia system, Solid State Ionics 53–56 (1992) 769–776.

[21] Y. Mizutani, M. Tamura, M. Kawai, O. Yamamoto, Development of high-performance electrolyte in SOFC, Solid State Ionics 72 (1994) 271–275.

[22] A Liu, J. Wang, C He, H Miao, Y. Zhang, W.G. Wang, Synthesis and characterization of $Gd_{0.1}Ce_{0.9}O_{1.95}$ nanopowder via an acetic-acrylic method, Ceram. Int. 39 (2013) 6229–6235.